Impact of climate change on Cannonsville Reservoir thermal structure in the New York City water supply

N. R. Samal, D. C. Pierson, E. Schneiderman, Y. Huang, J. S. Read, A. Anandhi and E. M. Owens

ABSTRACT

Global Circulation Model values of mean daily air temperature, wind speed and solar radiation for the 2081–2100 period are used to produce change factors that are applied to a 39 year record of local meteorological data to produce future climate scenarios. These climate scenarios are used to drive two separate, but coupled models: the Generalized Watershed Loading Functions-Variable Source Area model in order to simulate reservoir tributary inflows, and a one-dimensional reservoir hydrothermal model used to evaluate changes in reservoir thermal structure in response to changes in meteorological forcing and changes in simulated inflow. Comparisons between simulations based on present-day climate data (baseline conditions) and future simulations (change-factor adjusted baseline conditions) are used to evaluate the development and breakdown of thermal stratification, as well as a number of metrics that describe reservoir thermal structure, stability and mixing. Both epilimnion and hypolimnion water temperatures are projected to increase. Indices of mixing and stability show changes that are consistent with the simulated changes in reservoir thermal structure. Simulations suggest that stratification will begin earlier and the reservoir will exhibit longer and more stable periods of thermal stratification under future climate conditions.

Key words | climate change, mixing, New York City water supply, one-dimensional hydrodynamic model, thermal structure

N. R. Samal (corresponding author)
Y. Huang
CUNY Institute for Sustainable Cities,
Hunter College, City University of New York,
695 Park Avenue, New York, NY 10065,
USA
E-mail: *nsamal@hunter.cuny.edu*,
nsamal@dep.nyc.gov

N. R. Samal
Department of Civil Engineering,
National Institute of Technology Durgapur,
M.G. Avenue, Durgapur-713209, West Bengal,
India

D. C. Pierson
E. Schneiderman
New York City Department of Environmental Protection, 71 Smith Ave, Kingston, NY 12401,
USA

J. S. Read
University of Wisconsin-Madison,
Civil and Environmental Engineering,
Environmental Fluid Mechanics,
1415 Engineering Dr Rm 1261, Madison, WI 53706,
USA

A. Anandhi
Department of Agronomy,
Kansas State University, KS 66503,
USA

E. M. Owens
Upstate Freshwater Institute,
P.O. Box 506, Syracuse, NY 13214,
USA
and
Department of Civil and Environmental Engineering, Syracuse University,
Syracuse, NY 13244,
USA

SYMBOLS

CGCM	Canadian General Circulation Model
CMIP3	Coupled Model Intercomparison Project phase 3
ECHAM	European Centre Hamburg Model
GCM	General Circulation Model
GDP	Gross Domestic Product
GISS	Goddard Institute of Space Studies
GWLF-VSA	Generalized Watershed Loading Functions-Variable Source Area
IPCC	Intergovernmental Panel on Climate Change
SRES	Special Report on Emissions Scenarios
WDC	West Delaware Cannonsville
A	plane area of the reservoir basin
A_S	surface area of the lake

doi: 10.2166/wqrjc.2012.020

A_z	area of the lake at depth Z
c	specific heat of water
g	acceleration due to gravity
g^1	reduced gravity
K	turbulent diffusion coefficient
k_d	diffusion attenuation coefficient of solar radiation
k_s	surface heat transfer coefficient
Ln	lake number
L_s	lake fetch length
N	square root of the local buoyancy frequency
n	number of years
q_0	outflow per unit vertical distance
q_1	inflow per unit vertical distance
St	Schmidt stability
t	time
T	water temperature
T_b	bottom temperature
T_E	equilibrium temperature
T_s	surface temperature
T_1	inflow temperature
u_*	water friction velocity due to wind stress
V_T	total volume of reservoir
W	Wedderburn number
w	vertical velocity
y	year
z	vertical position (positive upward)
z_s	Secchi depth
z_D	maximum depth of the lake
z_e	depth to the top of the metalimnion
z_h	depth to the bottom of the metalimnion
z_v	depth to the center of volume of the lake
β	fraction of the net solar radiation
ΔT	temperature difference between surface and bottom temperature
φ_s	flux of solar radiation in the water column
φ_{so}	absorbed at the water surface
ρ	density of water
ρ_{epi}	average density of the epilimnion
ρ_h	density of hypolimnion
ρ_z	density of water at depth z
τ_w	wind shear on the water surface

INTRODUCTION

Lake and reservoir water temperatures respond to meteorological forcing, and these temperatures have a significant influence on the water quality and ecology of the corresponding aquatic ecosystems (Wetzel 1983; Samal *et al.* 2004a, b, 2010; Samal & Mazumdar 2005a, b). Changes in weather have direct effects on reservoir thermal characteristics, since reservoir thermal structure responds to the integrated effects of changes in the solar radiation, air temperature and wind speed. In order to describe the physical response of a reservoir to changes in external forcings, an adequate representation of the physical processes that structure water temperatures is important. These processes include vertical mixing, attenuation of penetrating radiation and stratification. Changes in local or regional climatic conditions, in particular, air temperature and the wind speed during winter have a significant influence on ice phenology (Scott & Huff 1996; Livingstone 1997; Skowron 2003; Borowiak & Baranczuk 2004), and variations in climate also influence the seasonal cycle of heat accumulation and loss in lakes and the duration and stability of summer thermal stratification. Further, the influence of large-scale climatic fluctuations on the regional coherence of surface water temperatures of European lakes has been demonstrated by Livingstone & Dokulil (2001). The impacts of ongoing climate change have been estimated to cause a systematic increase in lake surface temperature at a rate estimated to be about 0.02–0.035 °C per year, as described by Dabrowski *et al.* (2004). Huang *et al.* (2010) discussed the impact of net surface heat flux and wind speed on lake water surface temperature using a three-dimensional hydrodynamic model driven by both observed and modeled forcing at seasonal and synoptic time scales. The results revealed that differences in the simulations using observed and model forcing were mainly due to the difference in wind stress instead of the surface net heat fluxes. Various authors have suggested that surface water temperatures are highly correlated with regional-scale air temperatures, and that thermal characteristics (such as the onset and loss of stratification, intensity and duration of stratification, thermal stability and thermocline depth) are also related to regional

climatic conditions (Livingstone 2003; Coats *et al.* 2006). These physical controls influence the vertical distribution of nutrients and oxygen concentrations throughout the water column (Robertson & Imberger 1994; MacIntyre *et al.* 1999).

Experimental observations integrated with numerical modeling play a key role in describing the physical processes responsible for changes in stratification characteristics, since measurements and modeling can be used to test the sensitivity of the lakes and reservoirs to both observed and projected changes in the climate. Stefan *et al.* (1998) projected future lake water temperatures in response to a scenario of doubled atmospheric CO_2. The simulation results showed that ice formation was delayed and the ice cover period was shortened, resulting in differences in the seasonal patterns of water temperatures. A variety of one-dimensional models have been used to explore the potential impact of climate change on the dynamics of lakes and reservoirs, including studies undertaken by Hondzo & Stefan (1991), Markensten & Pierson (2007), Jones *et al.* (2009) and MacKay *et al.* (2009). These studies included sensitivity analyses run over long time scales to examine the imposed variability in thermal characteristics. Several studies have been carried out using climate-change scenarios obtained from General Circulation Models (GCMs), as described by Stefan *et al.* (1998), Arvola *et al.* (2010) and Lee *et al.* (2011). Different one- and two-dimensional hydrothermal models have been used for simulations in different regions of the globe (Peeters *et al.* 2002; Bell *et al.* 2006; Komatsu *et al.* 2006; Samal *et al.* 2009). A recent study on Lake Tahoe considering three GCMs show that the lake continues to be warmer and more stable with reduced mixing under future period (Sahoo *et al.* 2011). More examinations of variations in hydrothermal structure associated with forcing data derived from multiple GCM/emission scenarios in lakes and reservoirs are required.

The climatic processes influencing thermal structure also affect watershed hydrology, which, in turn, has a direct influence on the reservoir water balance and mixing. Vertical thermal profiles are affected differently under conditions of short versus long hydraulic retention times, also being dependent on the density-determined depth of the inflow current (Soballe *et al.* 1992). The combined effects of inflow and thermal structure modify the distribution of nutrients and phytoplankton and influence the overall mixing regime in lakes and reservoirs (Wetzel 1983; Thornton 1990; An 2001). Therefore, characteristics of watershed hydrology, such as streamflow volume and temperature, can play an important role in structuring the vertical distribution of water temperatures in a reservoir. As such, future changes in watershed hydrology have the potential to impact the water balance and hydrodynamics of a reservoir. Fortunately, integration of climate change, watershed dynamics and reservoir physics is possible, and the resulting changes can be simulated using a coupled system of watershed hydrologic and reservoir hydrothermal models.

In this study, downscaled GCM data at the watershed scale were used to produce reservoir-specific future climate scenarios. These scenarios allowed the application of a watershed hydrologic model to simulate inflows to a reservoir and a one-dimensional reservoir hydrothermal model to predict reservoir water temperatures under different emission scenarios. Comparisons between simulations based on present-day climate (baseline conditions) and future simulations (change-factor adjusted baseline conditions) are used to evaluate the development and breakdown of thermal stratification, as well as a number of metrics that describe reservoir thermal structure, stability and mixing.

MATERIALS AND METHODS

Study area and data acquisition

Cannonsville Reservoir (latitude 42°03′46′, longitude −75°22′24′) is located 190 km northwest of New York City, and is a drinking water reservoir owned and operated by the New York City Department of Environmental Protection. The reservoir receives inflows from a 1,160 km^2 watershed. Two major tributaries, the West Branch of the Delaware River and Trout Creek enter the two arms of the basin and drain 79 and 5% of the watershed area, respectively (Figure 1). The reservoir outflow occurs via a spillway located adjacent to the dam, and release ports at the base of the dam are used to control flow fractionation between downstream and one of the three drinking water intake structures.

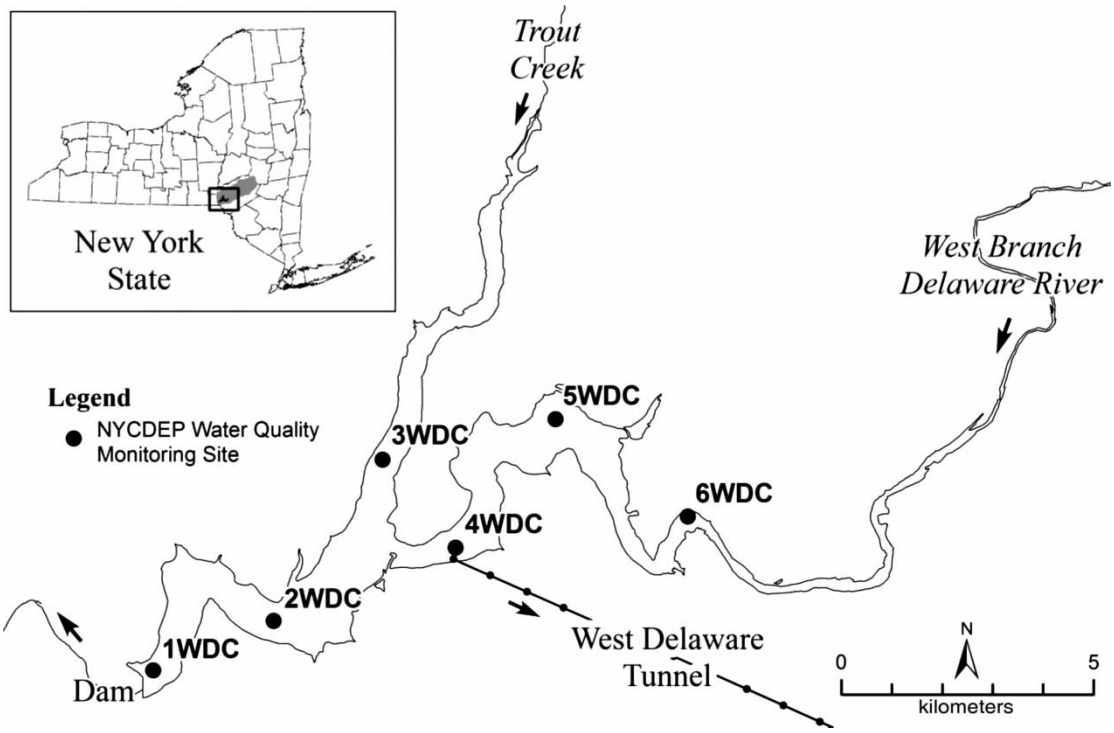

Figure 1 | Site map of Cannonsville Reservoir, showing monitoring sites, tributaries and dam location.

The morphometric details of the reservoir are presented in Table 1. The detailed descriptions of the reservoir's hydrology and operation have been published elsewhere (Owens *et al.* 1998). This reservoir had been originally classified as eutrophic (Effler *et al.* 1998), but as a result of improved waste water treatment and watershed management, it is now considered mesotrophic. In order to evaluate water quality management programs, Cannonsville Reservoir has been the focus of monitoring and modeling studies, and was an obvious choice for investigating the impact of climate change on the intrinsic dynamics of the reservoir, particularly in regards to nutrients and phytoplankton.

Table 1 | Reservoir characteristics

Reservoir characteristics	Value
Water surface area ($\times 10^6$ m^2)	19
Watershed area ($\times 10^6$ m^2)	1,178
Maximum length (m)	7,550
Maximum volume ($\times 10^6$ m^3)	366
Maximum depth (m)	52
Mean depth (m)	21
Shoreline development index	6
Residence time (days)	237
Storage capacity ($\times 10^4$ m^3)	36,226
Spillway elevation (m)	351

Model data

In order to drive the coupled modeling system used to produce simulations of reservoir thermal structure, two sources of meteorological data were used. To drive the one-dimensional reservoir hydrothermal model, data representative of the local conditions at the reservoir were needed. For this purpose, hydro-meteorological data from a 39 year record measured at local airports and later from a meteorological station at the reservoir dam were used. The on-site meteorological station was established in late 1994. Comparison of the 1995 measurements at the reservoir and at local airports indicated that the only significant differences on a given day were for wind speed and air temperature. As a result, the measured wind speed and air temperature at local airports were adjusted using a regression equation to estimate the wind

speed and air temperature at the reservoir (Gelda *et al.* 1998). In order to drive the Generalized Watershed Loading Functions-Variable Source Area (GWLF-VSA) watershed model that was used to simulate future inflow to the reservoir (described in detail in the next section), records of watershed-wide air temperature and precipitation were developed based on meteorological stations within and adjacent to the reservoir watershed boundaries. Watershed precipitation data input to GWLF-VSA were averaged based on Thiessen polygon weighting, and air temperatures are averaged using inverse distance weighting.

Historical records of watershed average, and local reservoir meteorology were used as inputs to our watershed and reservoir models, and the outcome of these simulations represent historical conditions of hydrological (inflow, water surface elevation, outflow, tributary temperature) and meteorological forcings (air temperature, dew point temperature, mean solar radiation, wind speed, cloud cover) on reservoir thermal structure. To verify the results of the reservoir hydrothermal model, we made use of temperature profiles that have been measured at six locations of the reservoir (Figure 1) at 1 m intervals from the surface to the near-bottom since 1992 in each ice-free month of the year.

Future climate scenarios

GCMs are advanced tools that simulate climatic conditions on earth for future periods based on the Intergovernmental Panel on Climate Change (IPCC) emission scenarios that account for possible future changes in anthropogenic forcings. Daily GCM simulation results from three GCMs were downloaded for the grid box closest to the centroid of the watershed. GCM simulations were obtained from the output of the three GCMs available from the World Climate Research Programme's Coupled Model Intercomparison Project phase 3 (CMIP3) dataset, including the Canadian Coupled General Circulation Model (CGCM), European Centre Hamburg Model (ECHAM GCM) and the Goddard Institute of Space Studies General Circulation Model (GISS GCM). These three models have all data needed to drive both the reservoir and watershed models used in this study, and also have these data available at the daily time step needed to run our models. In the initial phase of our work to evaluate the effects of climate change on the New York City water supply, we made use of the three models listed above. Ongoing work will make use of all models in the CMIP3 data archive that have the required data at a daily time step. The scenarios include a baseline scenario and three future emission scenarios (A1B, A2 and B1) for one future time slice (2081–2100). A brief description of the emission scenarios considered in this study is summarized in Table 2.

Daily GCM simulation results from the grid boxes overlying the New York City water supply watershed area were used to develop change factors that were in turn used to adjust local meteorological records to produce future scenarios to drive our models. Change factors were calculated from the differences between simulations of baseline (1981–2000) and future (2081–2100) time periods associated with the three GCMs and three emission scenarios. Single monthly change factors were developed, by pooling all of the data in a scenario for any given month and then

Table 2 | Brief explanation of the emission scenarios for the time slice (2081–2100) used in this study (modified from Anandhi *et al.* 2008)

Dataset	Description	IPCC name
720 ppm CO_2 maximum (SRES A1B)	Atmospheric CO_2 concentrations reach 720 ppm in the year 2100 in a world characterized by low population growth, very high GDP growth, very high energy use, low land-use changes, medium resource availability and rapid introduction of new and efficient technologies.	SRES A1B
850 ppm CO_2 maximum (SRES A2)	Atmospheric CO_2 concentrations reach 850 ppm in the year 2100 in a world characterized by high population growth, medium GDP growth, high energy use, medium/high land-use changes, low resource availability and slow introduction of new and efficient technologies.	SRES A2
550 ppm CO_2 maximum (SRES B1)	Atmospheric CO_2 concentrations reach 550 ppm in the year 2100 in a world characterized by low population growth, high GDP growth, low energy use, high land-use changes, low resource availability and medium introduction of new and efficient technologies.	SRES B1

calculating a scenario monthly mean. For air temperature, additive monthly change factors were calculated as the difference between the monthly means of a given future scenario and the baseline scenario. For all other meterological variables (precipitation, solar radiation and wind speed), monthly multiplicative change factors were calculated as the ratio of the mean monthly future to mean monthly baseline values. These change factors were then used to adjust a 39 year record of meteorological observations that was based on local measurements made at the reservoir (for the reservoir model), and another set of measurements that were representative of the entire reservoir watershed as a whole (for the watershed model). Additive change factors associated with a future scenario were added to the daily temperature data in the month corresponding to the change factor. In the case of multipicative factors, the daily data were multiplied by the change factor associated with a given month. The detailed method of producing the future climate-change data is described elsewhere (Anandhi *et al.* 2011). The variations of air temperature, wind speed and mean solar radiation for the baseline and other three emission scenarios are presented in Figure 2.

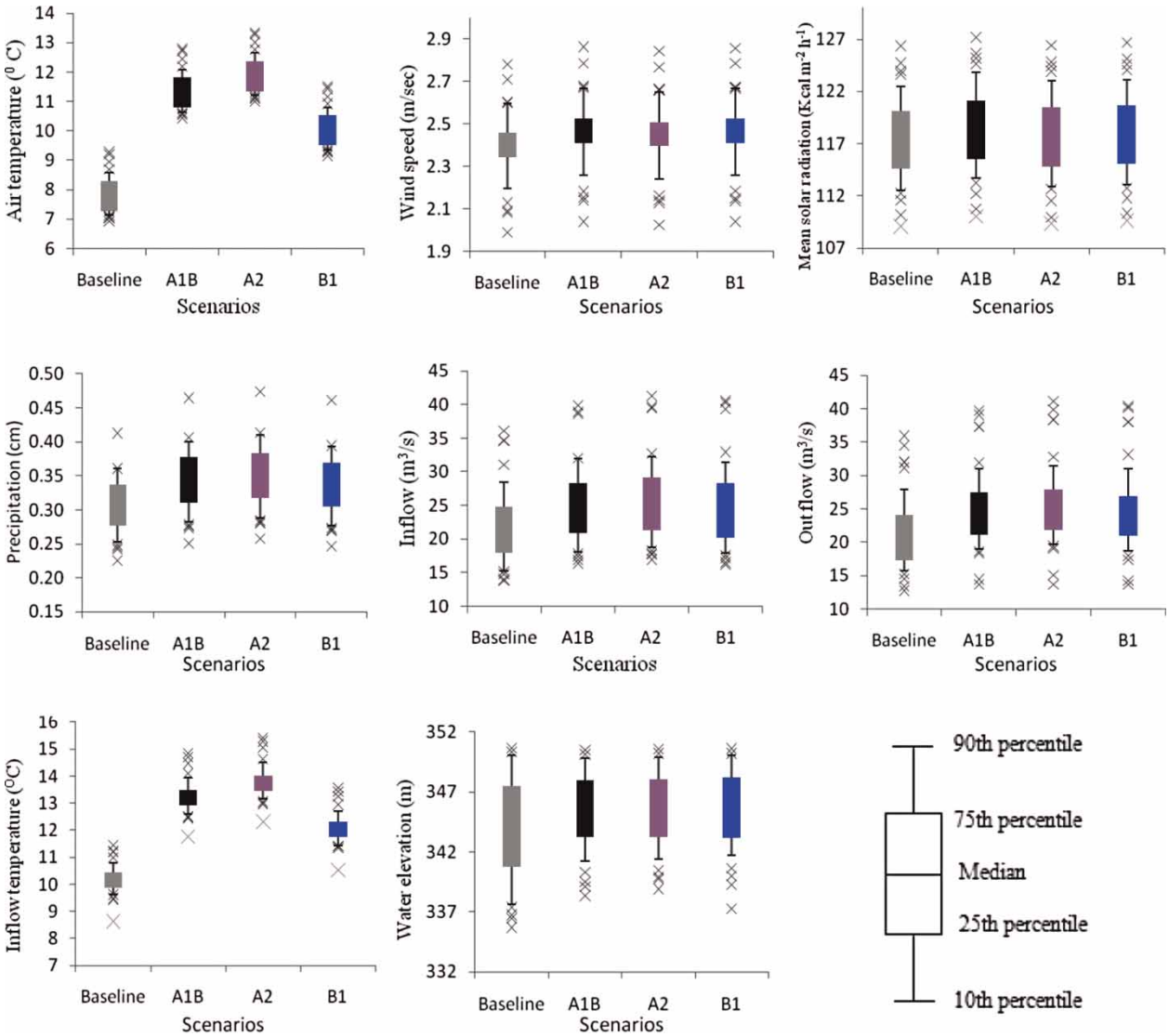

Figure 2 | Variation in the hydro-meteorological parameters for the baseline, A1B, A2 and B1 scenarios simulated using the CGCM3, ECHAM and GISS models.

Description of the modeling frame work

Future scenarios of air temperature and precipitation were used to drive both the GWLF-VSA watershed model to simulate the future reservoir inflows, and a one-dimensional hydrothermal model to simulate vertical water temperatures over historical data sets and future scenarios for the reservoir (Figure 3).

Reservoir model application

The one-dimensional reservoir model used to simulate thermal profiles under different climate scenarios consists of three components: (1) a hydrothermal sub-model (Owens 1998), (2) nutrient sub-models and (3) a phytoplankton sub-model based on the PROTECH model (Reynolds *et al.* 2001). In this paper, we focus solely on the output of the one-dimensional hydrothermal sub-model that is based on the heat conservation equations, water volume and turbulent kinetic energy (Harleman 1982; Samal *et al.* 2009) that assumes temperature, vertical water motion and mixing are all uniform in the horizontal plane and vary only in the vertical direction over time. These conservation equations are solved using an implicit integration method on a depth grid of 1 m with a time step of 30 minutes.

The one-dimensional heat conservation equation is given by:

$$\frac{\partial T}{\partial t} + W\frac{\partial T}{\partial z} = \frac{1}{A}\frac{\partial}{\partial z}\left(AK\frac{\partial T}{\partial z}\right) + \frac{1}{\rho cA}\frac{\partial}{\partial z}(A\varphi_s) + \sum\frac{q1}{A}(T_1 - T) \quad (1)$$

where T is water temperature, t is time, w is the vertical velocity, z is the vertical position (positive upward), A is the plane area of the reservoir basin, K is the turbulent diffusion coefficient, ρ and c are the density and specific heat of water, φ_s is the flux of solar radiation in the water column, q_1 is the inflow per unit vertical distance and T_1 is the inflow temperature.

The vertical velocity is determined from the areally averaged continuity equation for the basin given by:

$$w = \frac{1}{A}\int_0^z (q_1 - q_0)\mathrm{d}z \quad (2)$$

where q_0 is the outflow per unit vertical distance. The quantities q_1 and q_0 are determined by inflow and withdrawal/inflow that are described below.

The boundary condition at the reservoir water surface is:

$$-K\frac{\partial T}{\partial z} = (T - T_E)k_s + \frac{\beta\varphi_{so}}{\rho c} \quad (3)$$

where k_s is a surface heat transfer coefficient, T_E is the equilibrium temperature, β is the fraction of the net solar radiation, φ_{so} absorbed at the water surface. Expressions for water surface heat flux due to atmospheric radiation, back radiation, evaporation and conduction terms have been summed and linearized, resulting in the term $(T-T_E)$ k_s. During ice conditions, the expressions for k_s and T_E are modified to account for the presence of ice and to allow calculation of ice thickness (Ashton 1986; Owens & Effler 1996).

The flux of solar radiation in the water column φ_s is related to φ_{so} by:

$$\varphi_{so} = (1-\beta)\varphi_{so}e^{-k_d(z-z_s)} \quad (4)$$

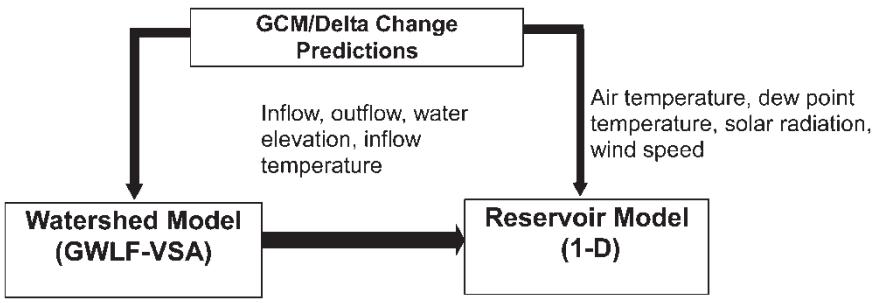

Figure 3 | Schematic diagram of model connections and dataflow used to simulate the reservoir thermal structure.

where k_d is the diffusion attenuation coefficient of solar radiation and z_s is the Secchi depth.

The turbulent vertical diffusivity, K, as incorporated in the conservation Equation (1), quantifies the mixing between adjacent layers in the water column. This model assumes that diffusion is driven by wind shear at the water surface and is damped in the water column by stable stratification. The vertical diffusivity is a function of both depth and time and is computed as:

$$K = C_H \frac{A_S\, u_*^3}{V_T N^r} \tag{5}$$

where C_H is an empirical coefficient (=0.0004), A_S is the surface area of the reservoir, u_* is the shear velocity due to wind stress at the water surface and set to zero with ice cover, V_T is the total reservoir volume, N is the square root of the local buoyancy frequency in the water column defined by $N^2 = -(g/\rho)(\partial\rho/\partial z)$ and r is an empirical coefficient (=0.3). The coefficients C_H and r were adjusted in calibration so that lower water temperatures agreed with measurements. The detailed verification and testing of the one-dimensional hydrothermal model for this Cannonsville Reservoir is described elsewhere (Owens 1998).

Watershed model

The watershed model used in this study is the GWLF-VSA model, which is a lumped-parameter model based on the original GWLF model (Haith & Schoemaker 1987) that simulates daily stream flow discharge and monthly sediment and nutrient loads at a watershed scale. Future climate scenarios derived from the same GCMs and using the same change-factor methodology were also used to drive the GWLF-VSA (Schneiderman *et al.* 2007) in order to simulate reservoir tributary inflow.

The Cannonsville Reservoir hydrothermal model is driven by site-specific bathymetric, hydrologic and meteorological data. The daily hydrologic parameters (inflow, water surface elevation, outflow, tributary temperature) are created by preprocessing the watershed model runs using a simple preprocessor program. The programs calculated inflow water temperature based on a simple regression model with air temperature, and when simulating inflows associated with future climate scenarios, the reservoir preprocessor also estimated reservoir spill, and if needed, adjusted reservoir operation to prevent drawdown to below critical levels.

Model calibration and validation

The model was calibrated using long-term (1986–2004) observed temperatures for the epilimnion and hypolimnion layers. Calibration was conducted to adjust the model parameters within their feasible range in order to minimize the root mean square error between measured and simulated temperature (Huang & Liu 2010). The same calibrated parameters were then used to predict the thermal profiles under future climate scenarios. The details of the feasible rage of model parameters and calibrated values are given in Table 3. Thermal profile data collected at the site of maximum depth (1WDC in Figure 1) during the years 1995–1999 are shown in Figure 4, and are compared to simulated data. It can be observed that predicted results are very similar to the observed data, and that the variations in surface temperature as well as epilimnetic and hypolimnetic temperature are well predicted by the model. Surface water temperature is an especially useful indicator of climate change since the meteorological forcing at the air–water interface is more sensitive to changes in surface meteorology.

Table 3 | Model parameters and calibrated values (Owens 1998; UFI 2001)

Sl no.	Model parameter	Calibrated values	Feasible range
1	Wind mixing	1.3000	1–1.5
2	Chlorophyll multiplier	0.0004	0–0.05
3	Diffusion exponent	0.3000	0.2–0.6
4	Maximum difference	5.0000	4.5–5.0
5	Evaporation constant	0.0004	0.003–0.005
6	Evaporation multiplier	0.0025	0.001–0.005
7	Atmospheric turbidity	2.2000	2–3
8	Surface adsorption fraction	0.4000	0.3–0.7
9	Ice albedo	0.4000	0.4–0.7
10	Ice extinction	2.0000	1.8–2.2
11	Ice transfer	0.0500	0.01–0.1
12	Ice emissivity	0.9500	0.9–0.99

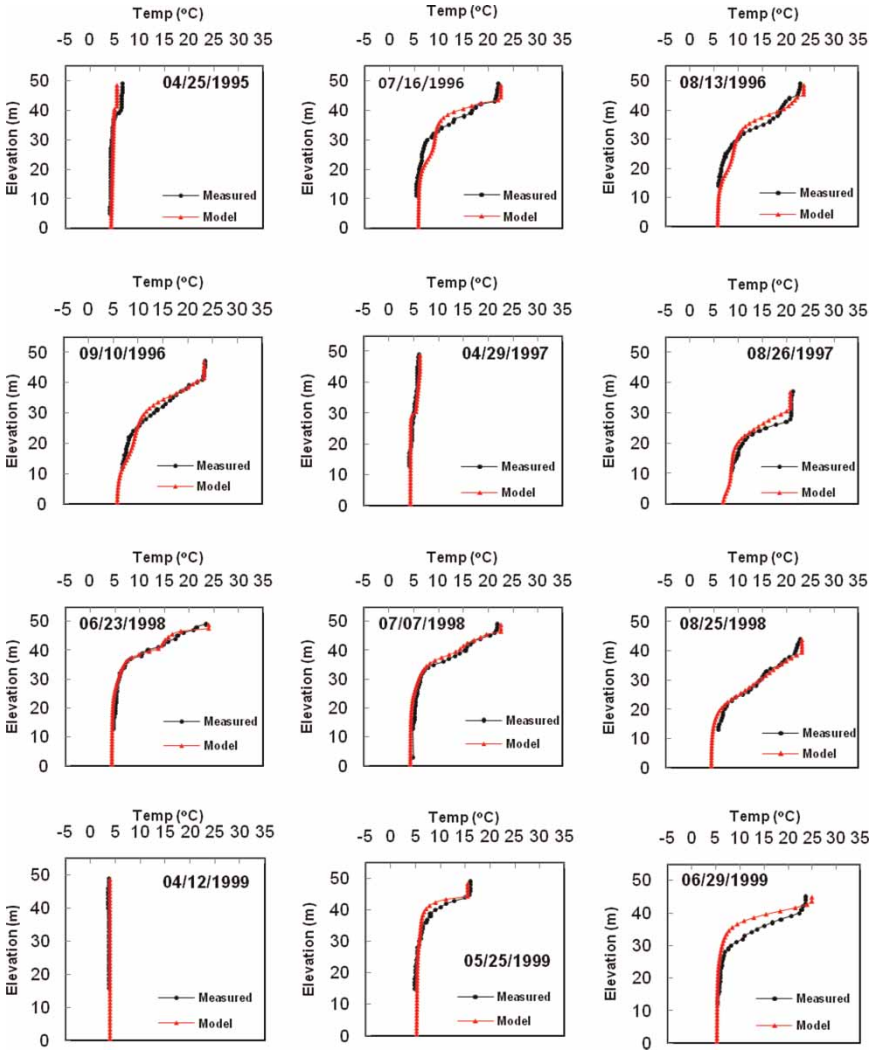

Figure 4 | Model comparison results of the vertical water temperature profiles in Cannonsville Reservoir.

Non-dimensional parameters and other metrics

Stratification and mixing indices (Schmidt stability, St (Jm^{-2}), bouyancy frequency (s^{-2}), thermocline depth (m), lake number (Ln) and Wedderburn number (W)) on a daily basis were derived from the daily simulated water temperature profiles and daily wind speed under the different climate scenarios (baseline, A1B, A2 and B1) using the lake analyzer program (Read *et al.* 2011) developed by the Global Lake Ecological Obervatory Network (http://www.gleon.org/).

Schmidt (1928) first defined St, which is the resistance to mechanical mixing due to the potential energy in the stratification of the water column. It was later modified by Hutchinson (1957), who described the strength of density stratification.

This stability index was further described by Idso (1973) to reduce the effects of lake volume on the calculation, resulting in the energy requirement on an areal basis:

$$\mathrm{St} = \frac{g}{A_S} \int_0^{z_D} (z - z_v)\rho_z A_z \partial z \tag{6}$$

where A_z is the area of the lake at depth z, g is the acceleration due to gravity, A_S is the surface area of the lake, ρ_z is the density of water at depth z, z_D is the maximum depth of the

lake and z_v is the depth to the center of volume of the lake, written as:

$$z_v = \int_0^{z_D} z A_z \partial z \Big/ \int_0^{z_D} A_z \partial z \tag{7}$$

St increases due to gradual warming of the surface waters, and as the so-called center of gravity of the system moves deeper into the water column as a result of vertical differences in density.

Ln, defined by Imberger & Patterson (1990), is an index of the dynamic stability of the water column accounting for the extent of deep turbulent mixing. A higher Ln indicates that the deep turbulent mixing is minimal, and lower values of Ln represent a higher potential for increased diapycnal mixing, which increases the vertical flux of mass and energy across the metalimnion through the mechanism of non-linear waves (MacIntyre *et al.* 2009).

Ln is given by:

$$\mathrm{Ln} = \frac{g \cdot \mathrm{St}_*(z_e + z_h)}{2\rho_h u_*^2 A_s^{3/2} z_v} \tag{8}$$

where $\mathrm{St}* = \mathrm{St} \cdot A_s/g$ is the Schmidt stability with Idso's (1973) surface area correction removed (Equation (5)) and z_e and z_h are the depths to the top and bottom of the metalimnion, respectively (see Read *et al.* 2011).

W, introduced by Thompson & Imberger (1980), describes the likelihood of upwelling events under stratified conditions.

W has frequently been used as a parameter to describe potential upwelling events in lakes (for example, Stevens & Lawrence 1997; MacIntyre *et al.* 2002; Lamont *et al.* 2004). W can be written as:

$$W = \frac{g' z_e^2}{u_*^2 L_s} \tag{9}$$

where $g' = g \cdot \Delta\rho/\rho_h$ is the reduced gravity due to the change in density ($\Delta\rho$) between the hypolimnion (ρ_h) and epilimnion, z_e is the depth to the base of the mixed layer, L_s is the lake fetch length and $u*$ is the water friction velocity due to wind stress, given by:

$$u* = \sqrt{\frac{\tau_w}{\rho_{epi}}} \tag{10}$$

where ρ_{epi} is the average density of the epilimnion and τ_w is the wind shear on the water surface.

Ln ~ 1 indicates that the wind is just sufficient to force the seasonal thermocline to be deflected to the surface at the upwind end of the lake (Robertson & Imberger 1994). When Ln > 15, stratification is strong (assumed in the case of deep lakes) and dominates the forces introduced by surface wind energy. For Ln < 1, stratification is weak with respect to wind stress, and the extensive turbulent mixing due to internal shear is predominant in the hypolimnion. $W \sim 1$ represents the threshold for upwelling of water located in the upper depths of the thermocline. When $W < 1$, full mixing can occur at the near-surface boundaries and in the interior due to non-linear waves (Boegman *et al.* 2005a, b). Recent laboratory measurements and analyses carried out by MacIntyre (2008) described that soliton formation and wave breaking near the boundaries of lakes is expected when $1 < W < 3$. The Brunt–Väisälä buoyancy frequency (N^2) is the maximum frequency at which the propagation of internal waves can be supported by the density stratification. This is equal to the frequency at which a water parcel would oscillate, when shifted vertically out of its equilibrium position. The buoyancy frequency defined by $N^2 = (g/\rho)(\partial\rho/\partial z)$, represents the local stability of the water column based on the resistance of the density gradient to the propagation of internal waves. Thermocline depth on a daily basis is estimated as the depth in the water column where the greatest density gradient with respect to depth is found.

RESULTS AND DISCUSSION

Climate scenarios

In the present study, data from three GCMs (CGCM3, ECHAM and GISS) were used to develop future climate

scenarios using a common change-factor methodology (Anandhi *et al.* 2011). A 39 year record of historical (baseline) meteorological data, and the future scenarios based on these historical data were in turn used to drive our reservoir hydrothermal model for baseline, and each of three emission scenarios (A1B, A2 and B1) for the 2081–2100 future periods. The spatial averaging associated with the large GCM grid cells make some form of downscaling a necessity. The simple change-factor approach used here is a compromise that allows small-scale variability inherent in the local records to be retained, while still producing future scenarios that reflect the broader changes suggested by the GCM data. Change-factor methodology does allow for changes in the seasonality of the meteorological data, since separate change factors are applied for each month. However, change-factor methodology does not allow the timing or frequency of meteorological events to change. Other methods of downscaling such as statistical downscaling or use of regional climate models are under investigation as part of our ongoing climate-change assessment. However, given that change-factor methodology is widely used (Anandhi *et al.* 2011), is simple to apply and not computationally demanding, it was a good choice for our first attempt to evaluate the impacts of climate change on reservoir thermal structure. The climate-change scenarios suggest substantial changes in future air temperatures, but very little change in solar radiation or wind speed. Median annual air temperature would increase by nearly 50% in the A2 scenario in comparison to baseline. Solar radiation and wind speed were less affected in the future scenarios, with the median annual changes in the range 1–3%, with no consistent differences between baseline and future scenarios.

Model simulations

Simulations using the reservoir hydrothermal sub-model allowed daily vertical profiles of simulated water temperature for the baseline and future climate scenarios to be produced. These were analyzed to examine changes in reservoir thermal structure and further processed using the lake analyzer tool to estimate the different reservoir hydrodynamics indices described above. Comparisons between simulations based on present-day climate data (baseline conditions) and future simulations (change-factor adjusted baseline conditions) are used to evaluate the development and breakdown of thermal stratification, as well as a number of metrics that describe reservoir thermal structure, stability and mixing. Simulations are presented as isopleths of temperature in Figure 5. These were created by averaging the daily temperature profiles (day 1–365) associated with the baseline simulation ($n = 39\,y$; n is the number of years and y is the year) and daily pooled data associated with the GCM scenarios ($n = 39\,y \times 3$ GCMs), and therefore represent the average pattern of thermal structure simulated as occurring over the baseline and future scenarios. The data analyzed here are affected by the combined effects of meteorological forcing on the resevoir itself, and changes in watershed inflows and reservoir water balance. Separate sensitivity runs were made to separate these two separate effects, and these showed that direct meteorological forcing was responsible for almost all simulated changes in reservoir thermal structure. Despite the small Effect of watershed inputs of reservoir thermal structure, we based the analysis below on simulations that accounted for both potential climate-change influences, in order to be complete, and since in the future, we plan to also examine the impacts of nutrient loading on reservoir water quality, which will clearly be impacted by processes operating in the watershed.

The temperature isopleths in Figure 5 show that in the future, the onset of stratification will begin earlier and end later, resulting in a longer period of stratification, particularly under the A1B and A2 emission scenarios that predict greater increases in atmospheric CO_2. The vertical extent of stratification is deeper, and epilimnetic and hypolimnetic temperatures are also warmer during the future scenarios, and again these changes are more pronounced for the A1B and A2 scenarios. The median depth of the thermocline is projected to increase by 25% for A1B and 37% for A2 scenario in Cannonsville Reservoir under future climate.

Comparing all climate scenarios shows that between 32 and 80% of a year undergoes stronger and deeper stratification, as defined by the temperature difference between surface and bottom ($\Delta T = T_s – T_b$) that ranged between 9 and 22 °C (Figure 6). Other investigations have discussed the sensitivity of surface and epilimnetic water temperature to warming trends as the surface water is exposed to incoming solar radiation and long-wave radiation from the

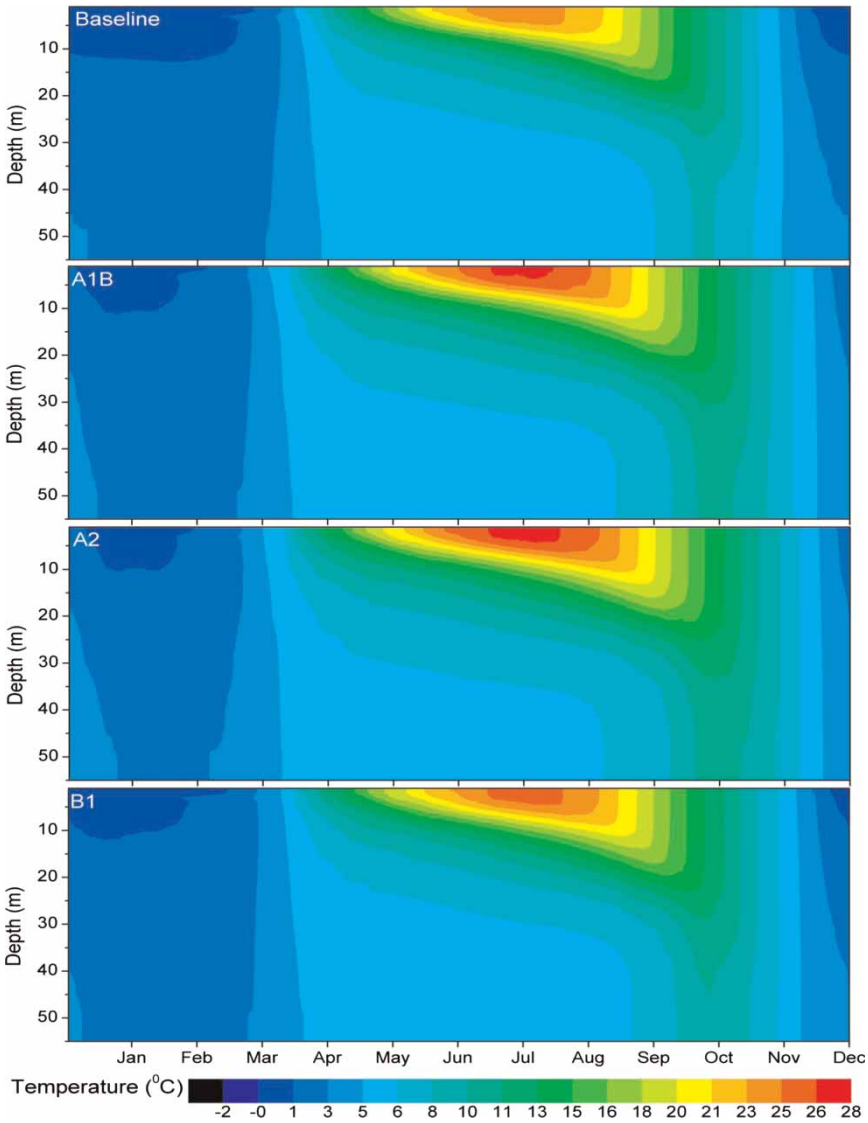

Figure 5 | Temperature isopleth diagrams for Cannonsville Reservoir under simulated baseline and future climate conditions.

atmosphere, whereas the hypolimnion is isolated from these sources of heat (Livingstone 2003; Peeters *et al.* 2007; Samal 2006; Boehrer & Schultze 2008; Hampton *et al.* 2008). Further, the warming and cooling of hypolimnetic temperature depends on lake morphometry (Gerten & Adrian 2000) and season (Ambrosetti & Barbanti 1999; Straile 2002).

In the scenarios projecting the higher levels of future emissions (A1B and A2), the mean surface water temperature is increased by approximately 10–12% and the near-bottom temperature is also substantially increased (Table 4). Hondzo & Stefan (1993) showed a reduction in hypolimnetic temperatures for some stratified North American lakes under future climate scenario. Our present findings suggest that the hypolimnetic temperature in this reservoir would increase in both A1B (12%) and A2 (14%) scenarios, and that this would occur concurrently with an earlier onset of stratification and longer duration of stratification (Figure 6; Table 4: 7 days for A1B and 12 days for A2). This implies that under a longer period of stratification, a larger amount of heat is transferred into deeper water under future climate conditions.

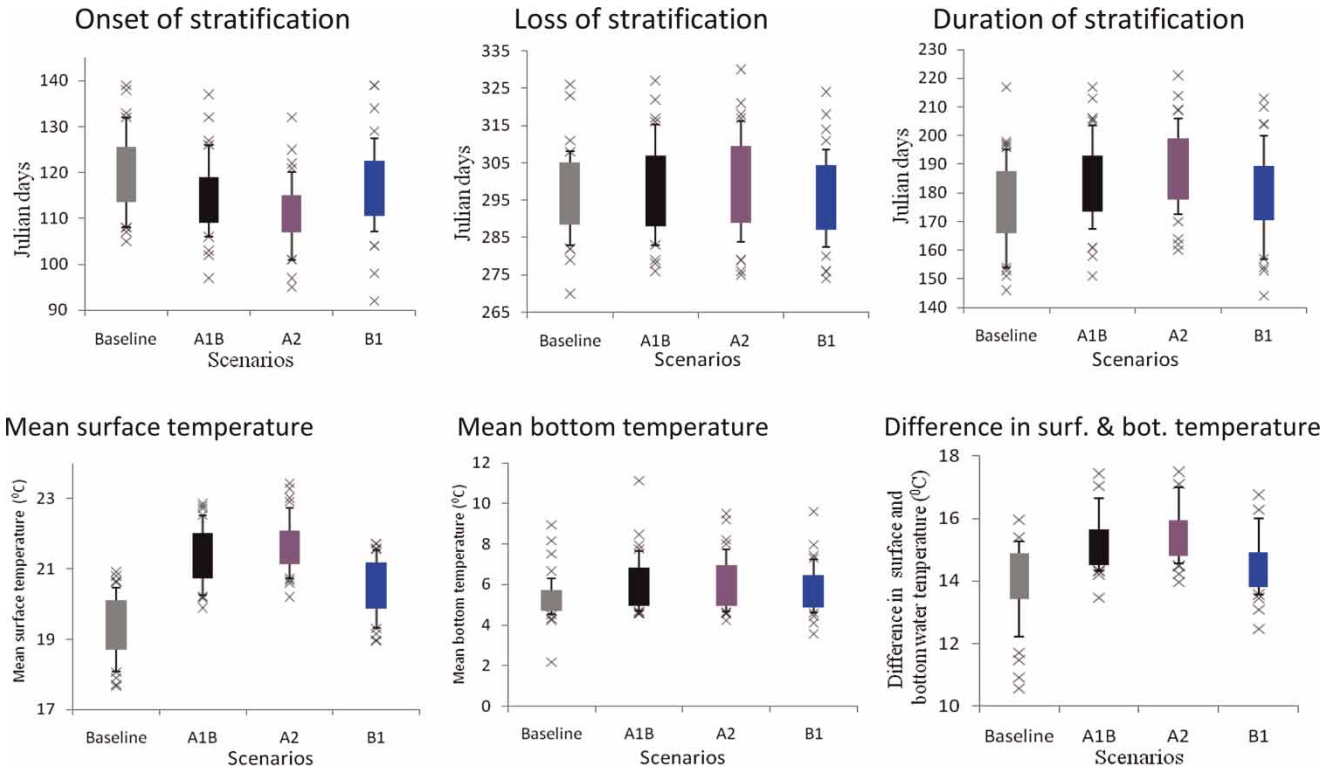

Figure 6 | Box plots created using daily data from the baseline scenario and pooled daily data from all GCM-derived scenarios. Measurements of water temperature are based on data during the period of thermal stratification only.

Table 4 | Changes in thermal stratification characteristics and reservoir hydrodynamic indices between baseline conditions and the future (2080–2100) time period

	Climate scenario	
Thermal characteristics and indices	**A1B**	**A2**
Length of stratification (days)*	07	12
Surface temperature (%)*	11	12
Near-bottom temperature (%)*	06	14
Reservoir indices		
Schmidt stability (%)	32	40
Buoyancy frequency (%)	29	38
Thermocline depth (%)	25	37
Lake number (%)	57	78
Wedderburn number (%)	86	134

*The values in the table are based on scenario averages of calculations made during the period of thermal stratification.

Reservoir indices

St increased in all future scenarios and was maximum in the A1B and A2 scenarios due to gradual warming of the surface waters, and the corresponding increases in vertical differences in density. Changes in buoyancy frequency suggest that the extent of deep turbulent mixing is reduced during the A1B and A2 scenarios as compared with present climate conditions. This is in agreement with the higher St during these scenarios (see Figure 7), since stronger stratification counteracts the forces introduced by the surface wind energy. A sensitivity test, which increased the daily wind speed by up to 6%, had only minor effects on simulated water temperature or St. The mean St calculated over the multiple years of the baseline and future scenario simulations was found to increase by 32% for A1B scenario and 40% for A2 scenario in the reservoir, whereas the buoyancy frequency showed an increase of 38% for A2 scenario in comparison to A1B scenario (29%).

W and Ln, which are based on water column stability, wind shear and basin dimension, explain the potential for convective or shear-driven mixing events during periods of thermal stratification, displayed a high amount of variability in the reservoir. Estimations of Ln and *W* strongly depend

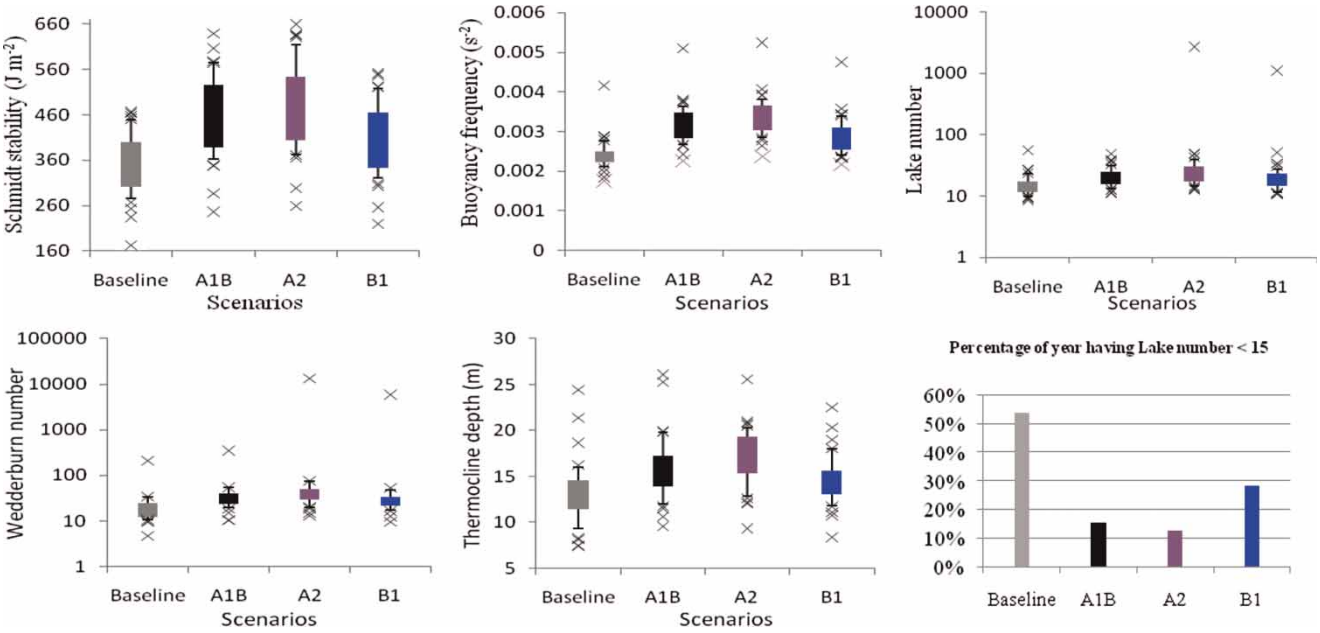

Figure 7 | Variations in hydrodynamic indices under baseline and future climate emission scenarios. Data in the figure are mean daily values calculated over the entire scenario period(s).

on the wind forcings, which are quite variable and less amenable to the change-factor downscaling used to produce the future climate scenarios. Despite this, both indices increased in value under the future climate scenarios in comparison to present conditions (see Table 4), suggesting that the reservoir will experience a stronger and longer period of stratification with a weakened likelihood of substantial diapycnal mixing during the stable stratification period. Low values of Ln tend to occur when the wind field is stronger during the transitions between warm and cold air masses in and around the reservoir area. The stability increased rapidly in this deep reservoir when Ln increased to a value more than 15 and the turbulence at the base of the mixed layer was suppressed. The percent of the year having $Ln < 15$ is estimated to decrease in A2 scenario, further indicating that climate change will lead to strong epilimnetic and hypolimnetic warming, and increased stratification of the water column under future emission scenarios.

Vertical variations in lake and reservoir water temperatures control the transport dynamics of dissolved and suspended particulate matter via density stratification. Accordingly, changes in the timing and strength of stratification can have a strong influence on water quality. The stable and the stronger stratification for the A1B and A2 scenarios could potentially reduce the extent of vertical mixing. Projections of warmer hypolimnetic water temperature and longer duration of stratification under future conditions are indicated by the metrics shown in Figure 7 and in Table 4. While hypolimnetic microbial activity will be influenced by a variety of factors, there is a general expectation that increased hypolimnetic temperature could potentially result in an increase in rates of hypolimnetic microbial activity occurring over a longer time and potentially increased depletion of hypolimnetic dissolved oxygen.

CONCLUSIONS

The simulation results of the effects of climate warming on the reservoir's thermal structure indicate that thermal structure is sensitive to projected future changes in meteorological conditions, with warmer future conditions resulting in earlier and longer periods of summer stratification, particularly under the A1B and A2 emission scenarios that predict greater increases in atmospheric CO_2. The one-dimensional model used in the present analysis performed well in predicting historical temperature

profiles (1966–2004), and also realistically simulated seasonal patterns of thermal stratification. Changes in the timing and intensity of stratification are important characteristics of all future scenarios. Comparing all climate scenarios shows that between 32 and 80% of a year stronger and deeper stratification will occur, as defined by the temperature difference between the surface and bottom ($\Delta T = T_s - T_b$) that ranged between 9 and 22 °C. Substantial increases in both surface and bottom temperatures were predicted under different future climate scenarios. The hypolimnetic temperature in this reservoir (located in Eastern USA) increased in both the A1B (12%) and A2 (14%) scenarios due to the early onset and longer duration of stratification (7 days for A1B and 12 days for A2) under future scenarios that are representative of the climate expected under different IPCC emission scenarios during the 2081–2100 future period. Such an increase in hypolimnetic temperature implies that increased amounts of heat will be transferred into deep water.

The mean St calculated over the entire period of simulation was greatest for A1B and A2 scenarios as compared to baseline and B1 scenarios. Future increases in Ln and W indicate that deep turbulent mixing will be reduced during A1B and A2 scenarios as compared with the present climate conditions, which is in agreement with higher St (St is a component in Ln). The stronger stratification dominates the forces introduced by the surface wind energy. The percent of the year having $Ln < 15$ is estimated to decrease in the future A2 scenarios, indicating that climate change leads to strong epilimnetic and hypolimnetic warming and increased stratification. When W and Ln are both large, the reservoir as a whole may be defined as a continuously stratified system with limited vertical mixing throughout the system.

These projections of warmer water temperature and longer duration of stratification under future conditions, as indicated by these metrics, could potentially result in an increase in the heat flux to the hypolimnion and reduced availability of dissolved oxygen. The application of a watershed model coupled to a hydrothermal model driven by the future climate scenarios has been shown to successfully simulate the variability in the hydrothermal characteristics, such as onset and decay of stratification, duration of summer stratification and in the magnitude and change in the thermocline depth. This is a useful tool for predicting the effects of climate change on the dynamics and coupling of lentic and lotic systems.

ACKNOWLEDGEMENTS

All support for this study was provided by the New York City Department of Environmental Protection (NYC DEP). The authors are grateful to Lorraine Janus, Chief, Watershed Water Quality Science & Research of New York City Department of Environmental Protection and Steven W. Effler, Director, Upstate Freshwater Institute, Syracuse, NY for their initial reviews of this paper. Also, the authors want to thank David Lounsbury and Donald Kent of the NYC DEP Water Quality Modeling Group for their help in map preparation and data collection. In addition, the authors would like to acknowledge the Global Lake Ecological Observatory Network (GLEON) for providing permission to use the Lake Analyzer tool.

REFERENCES

Ambrosetti, W. & Barbanti, L. 1999 Deep water warming in lakes: an indicator of climate change. *J. Limnol.* **58** (1), 1–9.

An, K. G. 2001 Seasonal patterns of reservoir thermal structure and water column mixis and their modifications by interflow current. *Korean J. Limnol.* **34** (1), 9–19.

Anandhi, A., Frei, A., Pierson, D. C., Schneiderman, E. M., Zion, M. S., Lounsbury, D. & Matonse, A. H. 2011 Examination of change factor methodologies for climate change impact assessment. *Water Resour. Res.* **47**, W03501.

Anandhi, A., Srinivas, V. V., Nanjundiah, R. S. & Kumar, D. N. 2008 Downscaling precipitation to river basin in India for IPCC SRES scenarios using support vector machine. *Int. J. Climatol.* **28**, 401–420.

Arvola, L., George, G., Livingstone, D. M., Järvinen, M., Blenckner, T., Dokulil, M. T., Jennings, E., Aongusa, C. N., Nõges, P., Nõges, T. & Weyhenmeyer, G. A. 2010 The impact of the changing climate on the thermal characteristics of lakes. In: *The Impact of Climate Change on European Lakes* (D. G. George, ed.), Aquatic Ecology Series 4. Springer Netherlands, Springer Science + Business Media B.V., pp. 85–101.

Ashton, G. D. 1986 *River and Lake Ice Engineering*. Water Resources Publications, Littleton, CO.

Bell, V. A., George, D. G., Moore, R. J. & Parker, J. 2006 Using a 1-D mixing model to simulate the vertical flux of heat and

oxygen in a lake subject to episodic mixing. *Ecol. Model.* **190**, 41–54.

Boegman, L., Ivey, G. N. & Imberger, J. 2005a The degeneration of internal waves in lakes with sloping topography. *Limnol. Oceanogr.* **50** (5), 1620–1637.

Boegman, L., Ivey, G. N. & Imberger, J. 2005b The energetics of large scale internal wave degeneration in lakes. *J. Fluid Mech.* **531**, 159–180.

Boehrer, B. & Schultze, M. 2008 Stratification of lakes. *Rev. Geophys.* **46**, RG2005.

Borowiak, D. & Baranczuk, J. 2004 Secular fluctuations of ice phenomena in Upper Radunia Lake, Kashubian Lakeland. *J. Limnol. Rev.* **4**, 17–24.

Coats, R., Perez-Losada, J., Schladow, G., Richards, R. & Goldman, C. 2006 The warming of Lake Tahoe. *Clim. Change* **76**, 121–148.

Dabrowski, M., Marszelewski, W. & Skowron, R. 2004 The trends and dependencies between air and water temperatures in lakes in northern Poland from 1961-2000. *Hydrol. Earth Syst. Sci.* **8** (1), 79–87.

Effler, S. W., Gelda, R. K., Perkins, M. G. & Matthews, D. A. 1998 Characteristics and origins of metalimnetic dissolved oxygen minima in a eutrophic reservoir. *Lake Reserv. Manage.* **14** (2–3), 332–343.

Gelda, R. K., Owens, E. M. & Effler, S. W. 1998 Calibration, verification and an application of a two-dimensional hydrothermal model [CE-QUAL-W2(t)] for Cannonsville Reservoir. *Lake Reserv. Manage.* **14** (2–3), 186–196.

Gerten, D. & Adrian, R. 2000 Climate-driven changes in spring plankton dynamics and the sensitivity of shallow polymictic lakes to the North Atlantic Oscillation. *Limnol. Oceanogr.* **45**, 1058–1066.

Haith, D. A. & Shoemaker, L. L. 1987 Generalized watershed loading functions for stream flow nutrients. *Water Resour. Bull.* **23** (3), 471–478.

Hampton, S. E., Izmest'Eva, L. R., Moore, M. V., Katz, S. L., Dennis, B. & Silow, E. A. 2008 Sixty years of environmental change in the world's largest freshwater lake – Lake Baikal, Siberia. *Glob. Change Biol.* **14**, 1947–1958.

Harleman, D. R. 1982 Hydrothermal analysis of lakes and reservoirs. *J. Hydr. Eng.* **108**, 302–325.

Hondzo, M. & Stefan, H. G. 1991 Three case studies of lake temperature and stratification response to warmer climate. *Water Resour. Res.* **27** (8), 837–1846.

Hondzo, M. & Stefan, H. G. 1993 Regional water temperature characteristics of lakes subjected to climate change. *Clim. Change* **24**, 187–211.

Huang, Y. T. & Liu, L. 2010 Multiobjective water quality model calibration using a hybrid genetic algorithm and neural network-based approach. *J. Environ. Eng.* **136** (10), 1020–1031.

Huang, A., Rao, Y. R. & Lu, Y. 2010 Evaluation of a 3-D hydrodynamic model and atmospheric forecast forcing using observations in Lake Ontario. *J. Geophys. Res.* **115**, C02004.

Hutchinson, G. E. 1957 *A Treatise on Limnology: Geography, Physics and Chemistry*, Vol. 1. John Wiley & Sons, Inc., New York, pp. 510–511.

Idso, S. B. 1973 On the concept of lake stability. *Limnol. Oceanogr.* **18**, 681–683.

Imberger, J. & Patterson, J. 1990 Physical limnology. *Adv. Appl. Mech.* **27**, 303–475.

Jones, I., Sahlberg, J. & Persson, I. 2009 Modelling the impact of climate change on the thermal characteristics of lakes. In: *The Impact of Climate Change on European Lakes* (D. G. George, ed.), Aquatic Ecology Series 4. Springer Netherlands, Springer Science + Business Media B.V., pp. 103–120.

Komatsu, E., Fukushima, T. & Shiraishi, H. 2006 Modeling of P-dynamics and algal growth in a stratified reservoir – mechanisms of P-Cycle in water and interaction between overlying water and sediment. *Ecol. Model.* **197**, 331–349.

Lamont, G., Laval, B., Pawlowicz, R., Pieters, R. & Lawrence, G. A. 2004 Physical mechanisms leading to upwelling of anoxic bottom water in Nitinat Lake. In: *17th ASCE Engineering Mechanisms Conference*, June 13–16, 2004. University of Delaware, Newark, Delaware, EEUU, 8 pp.

Lee, H. W., Kim, E. J., Park, S. S. & Choi, J. H. 2011 Effects of climate change on the thermal structure of lakes in the Asian Monsoon Area. *Clim. Change* **112**, 859–880.

Livingstone, D. M. 1997 Break-up dates of Alpine lakes as proxy data for local and regional air temperatures. *Clim. Change* **37**, 407–439.

Livingstone, D. M. 2003 Impact of secular climate change on the thermal structure of a large temperate central European lake. *Clim. Change* **57**, 205–225.

Livingstone, D. M. & Dokulil, M. T. 2001 Eighty years of spatially coherent Austrian lake surface water temperatures and their relationship to regional air temperature and the North Atlantic Oscillation. *Limnol. Oceanogr.* **46** (5), 1220–1227.

MacIntyre, S. 2008 Describing fluxes within lakes using temperature arrays and surface meteorology. *Verh. Internat. Verein. Limnol.* **30** (3), 339–344.

MacIntyre, S., Flynn, K. M., Jellison, R. & Romero, J. R. 1999 Boundary mixing and nutrient fluxes in Mono Lake, California. *Limnol. Oceanogr.* **44**, 512–529.

MacIntyre, S., Romero, J. R. & Kling, G. W. 2002 Spatial-temporal variability in surface layer deepening and lateral advection in an embayment of Lake Victoria, East Africa. *Limnol. Oceanogr.* **47**, 656–671.

MacIntyre, S., Fram, J. P., Kushner, P. J., Bettez, N. D., O'Brien, W. J., Hobbie, J. E. & Kling, G. W. 2009 Climate-related variations in mixing dynamics in an Alaskan arctic lake. *Limnol. Oceanogr.* **54**, 2401–2417.

MacKay, M. D., Neale, P. J., Arp, C. D., De Senerpont Domis, L. N., Fang, X., Gal, G., Johnk, K. D., Kirillin, G., Lenters, J. D., Litchman, E., MacIntyre, S., Marsh, P., Melack, J., Mooij, W. M., Peeters, F., Quesada, A., Schladow, S. G., Schmid, M., Spence, C. & Stokesr, S. L. 2009 Modeling lakes

and reservoirs in the climate system. *Limnol. Oceanogr.* **54** (6, part 2), 2315–2329.

Markensten, H. & Pierson, D. 2007 Weather driven influences on phytoplankton succession in a shallow lake during contrasting years: application of PROTBAS. *Ecol. Model.* **207**, 128–136.

Owens, E. M. 1998 Development and testing of one-dimensional hydrothermal models of Cannonsvile reservoir. *Lake Reserv. Manage.* **14** (2–3), 172–185.

Owens, E. M. & Effler, S. W. 1996 Modelling the impacts of a proposed hypolimnetic wastewater discharge on lake stratification and mixing in Onondaga lake. *Lake Reserv. Manage.* **12**, 195–206.

Owens, E. M., Gelda, R. K., Effler, S. W. & Hassett, J.-M. 1998 Hydrologic analysis and model development for Cannonsville Reservoir. *Lake Reserv. Manage.* **14** (2–3), 140–151.

Peeters, F., Livingstone, D. M., Goudsmit, G.-H., Kipfer, R. & Forster, R. 2002 Modeling 50 years of historical temperature profiles in a large central European lake. *Limnol. Oceanogr.* **47**, 186–197.

Peeters, F., Straile, D, Lorke, A. & Ollinger, D. 2007 Turbulent mixing and phytoplankton spring bloom development in a deep lake. *Limnol. Oceanogr.* **52** (1), 286–298.

Read, J. S., Hamilton, D. P., Jones, J. D., Muraoka, K., Winslow, L. A., Kroiss, R., Wu, C. H. & Gaiser, E. 2011 Derivation of lake mixing and stratification indices from high-resolution lake buoy data. *Environ. Model. Softw.* **26** (11), 1325–1336.

Reynolds, C. S., Irish, A. E. & Elliott, J. A. 2001 The ecological basis for simulating phytoplankton responses to environmental change (PROTECH). *Ecol. Model.* **140**, 271–291.

Robertson, D. M. & Imberger, J. 1994 Lake number, a quantitative indicator of mixing used to estimate changes in dissolved oxygen. *Int. Revue Ges. Hydrobiol.* **79** (2), 159–176.

Sahoo, G. B., Schladow, S. G., Reuter, J. E. & Coats, R. 2011 Effects of climate change on thermal properties of lakes and reservoirs, and possible implications. *Stoch. Environ. Res. Risk Assess.* **25**, 445–456.

Samal, N. R. 2006 Study of Morphometry and Hydrothermal Analysis of Tropical Shallow Lake. PhD Thesis, School of Water Resources Engineering, Jadavpur University, Kolkata, West Bengal, India.

Samal, N. R. & Mazumdar, A. 2005a Artificial boundary effect on primary productivity of the littoral garden. *J. Environ. Prot.* **25** (4), 334–338.

Samal, N. R. & Mazumdar, A. 2005b Management of lake ecosystem. *J. Ekologia* **3** (2), 123–130.

Samal, N. R., Mazumdar, A., Johnk, K. D. & Peeters, F. 2009 Assessment of ecosystem health of tropical shallow waterbodies in eastern India using turbulence model. *J. Aqua. Ecosys. Health Manage. Soc.* **12** (2), 215–225.

Samal, N. R., Roy, P. K., Biswas, M. & Mazumdar, A. 2010 Summer thermal stratification: an indicator of water pollution in shallow lake. *J. Chem. Eng., Instit. Eng. (India)*, **90**, 37–43.

Samal, N. R., Roy, D., Mazumdar, A. & Bose, B. 2004a Seasonal response of water temperature of Rabindra Sarobar, the National Lake, in relation to pH, dissolved oxygen, biochemical oxygen demand and chemical oxygen demand. *J. Public Health Eng.* **2**, 39–42.

Samal, N. R., Roy, D., Mazumdar, A. & Bose, B. 2004b Influence of thermal stratification on dissolved oxygen in Subhas Sarobar, Kolkata. *J. Curr. Sci.* **7** (1), 259–266.

Schmidt, W. 1928 Ober Temperatur und Stabilitaitsverhaltnisse von Seen (Upper temperature and stability ratio of lakes). *Geogr. Ann.* **10**, 145–177.

Schneiderman, E. M., Steenhuis, T. S., Thongs, D. J., Easton, Z. M., Zion, M. S., Neal, A. L., Mendoza, G. F. & Walter, M. T. 2007 Incorporating variable source area hydrology into the curve number based Generalized Watershed Loading Function model. *Hydrol. Process.* **21**, 3420–3430.

Scott, R. W. & Huff, F. A. 1996 Impacts of the Great Lakes on regional climate conditions. *J. Great Lakes Res.* **22**, 845–863.

Skowron, R. 2003 Ice sheet in the lakes of Polish lowland. Distribution, differences and trends. *Limnol. Rev.* **3**, 205–212.

Soballe, D. M., Kimmel, B. L., Kennedy, R. H. & Gaugush, R. F. 1992 Lentic systems: reservoirs. In: *Biodiversity of the Southeastern United States Aquatic Communities* (C. T. Hackney, S. M. Adams & W. H. Martin, eds). Wiley, New York.

Stefan, H. G., Fang, X. & Hondzo, M. 1998 Simulated climate change effects on year round water temperatures in temperate zone lakes. *Clim. Change* **40**, 547–576.

Stevens, C. & Lawrence, G. A. 1997 Estimation of wind-forced internal seiche amplitudes in lakes and reservoirs, with data from British Columbia, Canada. *Aquat. Sci.* **58**, 1–20.

Straile, D. 2002 North Atlantic Oscillation synchronizes food-web interactions in central European lakes. *Proc. R. Soc. B Biol. Sci.* **269**, 391–395.

Thompson, R. O. & Imberger, J. 1980 Response of a numerical model of a stratified lake to wind stress. In: Stratified flows. Proc. 2nd Int. Symp. Trondheim, 1: 562–570.

Thornton, K. W. 1990 Perspectives on reservoir limnology. In: *Reservoir Limnology: Ecological Perspectives* (K. W. Thornton, B. L. Kinnel & F. E. Payne, eds). A Wiley-Interscience publication, John Wiley & Sons Ltd, Chichester.

Upstate Freshwater Institute (UFI) 2001 *Calibration, Verification of a One-Dimensional Hydrothermal and Eutrophication Model for Catskill/Delaware Reservoirs*. UFI, New York.

Wetzel, R. G. 1983 *Limnology*. W. B. Saunders Co., Philadelphia.

First received 2 March 2012; accepted in revised form 14 September 2012